Tuning Kerr-Soliton Frequency Combs to Atomic Resonances

Su-Peng Yu,[1,2,*] Travis C. Briles,[1,2] Gregory T. Moille,[3,4] Xiyuan Lu,[3,4] Scott A. Diddams,[1,2] Kartik Srinivasan,[3] and Scott B. Papp[1,2]

[1] *Time and Frequency Division, NIST, 325 Broadway, Boulder, CO 80305, USA*

[2] *Department of Physics, University of Colorado, 390 UCB, Boulder, CO 80309, USA*

[3] *Microsystems and Nanotechnology Division, NIST, 100 Bureau Dr, Gaithersburg, MD 20899, USA*

[4] *Maryland Nanocenter, University of Maryland, 225 Paint Branch Dr, College Park, MD 20740, USA*

Frequency combs based on nonlinear optical phenomena in integrated photonics are a versatile light source that can explore new applications, including frequency metrology, optical communications, and sensing. We demonstrate robust frequency-control strategies for near-infrared, octave-bandwidth soliton frequency combs created with nanofabricated silicon nitride ring resonators. Group-velocity-dispersion engineering allows operation with a 1064-nm pump laser and generation of dual-dispersive-wave frequency combs linking wavelengths approximately between 767 and 1556 nm. To tune the mode frequencies of the comb, which are spaced by 1 THz, we design a photonic chip containing 75 ring resonators with systematically varied dimensions and we use a thermo-optic tuning range of 50 °C. This single-chip frequency-comb source provides access to every wavelength, including those critical for near-infrared atomic spectroscopy of rubidium, potassium, and cesium. To make this possible, solitons are generated consistently from device to device across a single chip with use of rapid pump-frequency sweeps that are provided by an optical modulator.

I. INTRODUCTION

Recently, there has been much effort to develop chip-scale and integrated-photonics light sources and devices through nonlinear optics [1]. These have ranged from the development of ultrastable cw lasers based on stimulated Brillouin scattering [2,3] to metrology with frequency combs based on supercontinuum generation in photonic waveguides [4,5] to dissipative-Kerr-soliton (DKS) formation in microresonators [6,7]. Such soliton microcombs exhibit interesting nonlinear optical phenomena, including breathing oscillations [8–10], dark-pulse formation [11], and soliton crystallization [12], and have enabled diverse applications such as communications [13] and optical frequency synthesis [14]. DKS combs have been demonstrated with a variety of materials, including fused-silica fiber and microresonators [15,16], crystalline magnesium fluoride [17], and silicon nitride (Si_3N_4) [18–20]. Si_3N_4 is an appealing material for broad-bandwidth combs due to its moderately high Kerr nonlinearity and low optical propagation loss. Additionally, it is compatible with standard lithographic fabrication techniques, allowing reliable fabrication of resonators and integration with other photonic elements [1], providing a path for broadband,

low-power-consumption frequency combs on a photonic chip [21].

Realizing DKS frequency combs that interface with optical atomic transitions opens up timekeeping and other measurement applications. However alkali or alkaline-earth atomic resonances are largely prevalent in the 700–1000-nm spectral region, whereas many DKS experiments were performed in the 1550-nm band due to the availability of pump lasers, optical amplifiers, filters, detectors, and other components. Previous optical clock demonstrations with soliton microcombs were pumped at 1550 nm [22,23], and required second-harmonic generation to access atomic transitions. Moreover, atomic transitions are spectrally narrow and thus require fine-tuning of a frequency comb to reach resonance.

A central facet of designing DKS combs for the near-infrared (NIR) region [24] is that the very high microwave-to-terahertz repetition frequencies of microcombs and their ultrabroad-bandwidth spectra are almost exclusively determined by the geometry of the devices. A recipe has emerged to design and realize soliton microcombs at 1550 nm for some applications such as optical frequency synthesis [20]. The first step in designing the soliton spectrum is to select device geometries with anomalous group-velocity dispersion (GVD) near the chosen pump wavelength [25]. A second step is to design higher-than-second-order GVD

---

*yuadam.prime@gmail.com

contributions for the generation of dispersive waves (DWs) [26], which lead to a localized increase in optical power at the edges of the soliton spectrum. A third step is tuning the carrier-envelope offset frequency of the soliton microcomb for compatibility with electronic detection with available high-speed photodetectors with bandwidth of 20 GHz or less.

Here we explore frequency control and tuning of octave-spanning, NIR soliton microcombs pumped at 1064 nm, toward use in atomic spectroscopy. We demonstrate a combination of GVD control of the comb's spectrum and thermo-optic frequency tuning for a single-chip solution to interface with rubidium (780 nm), cesium (852 nm), and potassium (767 nm) atoms. The advantage of a 1064-nm pump laser is that it bisects the frequency span between telecom wavelengths (1300–1600 nm) and the resonance wavelengths of atomic species that are commonly used for atomic clocks, such as strontium (699 nm) and calcium ion (729 nm) [27–29]. Our soliton microcomb provides up to 0.3 μW per mode over the 760–900 nm range of interest for atomic spectroscopy, and also a few microwatts per mode in the telecom bands. The comb is pumped with standard 1064-nm-laser technology, and we demonstrate high coherence with the soliton microcomb through detection of its 1-THz repetition frequency and f -2f measurements.

II. SOLITON-MICROCOMB DESIGN

The photonic chip resonators in this study are Si_3N_4 microring resonators embedded in a silicon dioxide cladding. A ring radius of 22.5 μm (center of waveguide) is chosen to give a free spectral range (FSR) of approximately 1 THz, which reduces the comb operating power [20]. The devices are fabricated at wafer scale by Ligentec using LPCVD of stoichiometric silicon nitride, deep-UV stepper lithography, dry chemical etching, and separation to individual chips. Broadband, weakly anomalous GVD is created near the 1064-nm pump-laser wavelength by design of the resonator dimensions; namely, the Si_3N_4 layer thickness and the resonator waveguide width (W). GVD simulations for resonators with a Si_3N_4 layer thickness of 667 nm and W of 810, 850, and 890 nm illustrate the soliton-microcomb design process; see the top panel in Fig. 1(a). We indicate the telecom bands (1500–1600 nm) and the NIR range relevant for rubidium atomic spectroscopy (778–795 nm) by vertical gray boxes.

Our resonators also support the generation of DWs that extend the soliton spectrum outside the anomalous-GVD region. The emitted DWs correspond approximately to the wavelengths of zero integrated dispersion, D_{int} [18]. The integrated dispersion is equivalent to the detuning of the cold-resonator frequencies ν_μ from an equidistant grid centered at the pump-laser frequency and spaced by the FSR
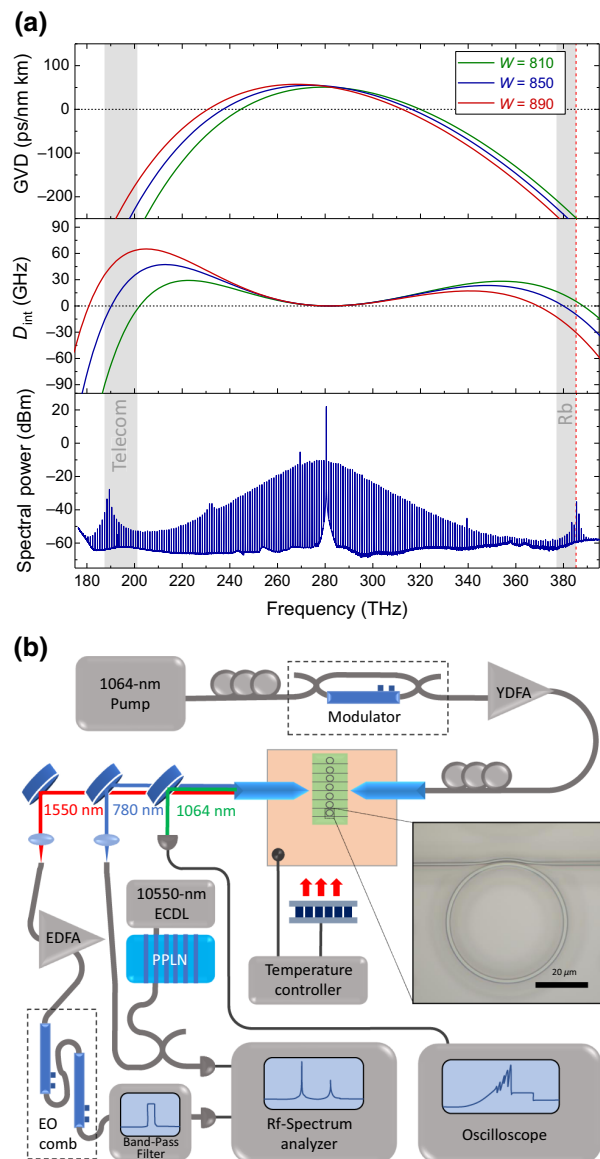

(a)

(b)

FIG. 1. Resonator dispersion design and experimental setup. (a) The calculated GVD profile (top) and integrated modal dispersion (middle) for ring resonators with material thickness of 667 nm, radius of 22.5 μm, and W of 810, 850, and 890 nm. The experimentally generated single-soliton spectrum from the device with W of 850 nm (bottom) has its strongest SDW line aligned with the Rb two-photon transition (dashed red line). (b) The experimental setup for soliton generation and comb diagnostics. An external-cavity diode laser (ECDL) is coupled to a Mach-Zehnder intensity modulator, amplified in an ytterbium-doped fiber amplifier (YDFA), and coupled into the photonic chip using lensed fibers and precision positioning stages. The generated comb light is separated into spectral bands centered at 780, 1064, and 1550 nm for subsequent diagnostics. Each branch can be monitored in real time or heterodyned with local oscillators with local oscillators. The notch filter used in the 1064-nm branch to reject pump light when soliton generation is being monitored is not shown. The long-wavelength-DW branch is amplified with an erbium-doped fiber amplifier (EDFA) to provide optical power for further measurement steps. EO, electro-optic; PPLN, periodically poled lithium niobate.

about the pump-laser frequency:

$$D_{\text{int}}(\mu) = \nu_\mu - \left(\nu_p - \mu \times \frac{D_1}{2\pi} \right), \qquad (1)$$

where ν_p is the pump-laser frequency, $D_1/2\pi$ is the resonator FSR near the pump-laser frequency, and μ is an integer indexing the resonances relative to the pumped mode $\mu = 0$. This quantity, given in gigahertz, is plotted in the middle panel in Fig. 1(a) for the three corresponding traces in the top panel. Increasing the W leads to an overall redshift of the GVD profile as well as the wavelengths of $D_{\text{int}} = 0$. Since both the device layer thickness and the W affect the GVD profile, we can quasi-independently design and control the peak wavelength of the two DWs.

The linear approximation for the DW wavelengths given by $D_{\text{int}}(\mu) = 0$ ignores higher-order effects arising from soliton self-phase modulation [30]. However, it is a reasonable criterion for predicting the performance of resonator designs given the fabrication tolerances of approximately 5 nm in device layer thickness and approximately 20 nm in pattern dimensions, including effects of waveguide sidewall angle. These small deviations are accounted for by the fabrication of resonators of various Ws, stepped by tens of nanometers, on a single chip. We design chips composed of approximately 75 individual ring resonators to systematically cover the microcomb design space.

The bottom panel in Fig. 1(a) shows the result of our controllably taking advantage of the microcomb design space in Si_3N_4. The soliton-microcomb spectrum that we present features a long-wavelength DW in the telecom band and a short-wavelength DW with its strongest line aligned with the Rb two-photon clock transition at 778 nm [31–33].

III. OPTICAL MEASUREMENT

The setup we use for our experiments is shown in Fig. 1(b). In particular, the apparatus is composed of elements for soliton-microcomb generation and thermo-optic tuning, and for coherence measurements of the soliton microcomb's carrier-envelope-offset frequency and repetition frequency. The pump laser we use is an external-cavity diode laser, providing coarse tuning from 1020 to 1070 nm to address a few of the TE1 ring-resonator modes that are spaced by 1 THz.

To provide laser light to our resonators, coupling waveguides are fabricated in the silicon nitride device layer. Inverse tapering of the coupling waveguide at chip edge enables insertion loss of approximately 3 dB per facet from standard lensed fibers. A "pulley" design [20,34,35] for the coupling waveguide achieves adequate coupling rates for low-power operation of the comb and also at the edges of the spectrum for output coupling of the dispersive waves. We include a variation in the coupling gap between the

pulley coupler and the resonator to achieve critical coupling; namely, to set the coupling strength between the resonator and the coupling waveguide to match the internal loss of the resonator. This coupling condition maximizes the intraresonator power for a given pump power, reducing the pump power required to support soliton microcombs. We extract information on the intrinsic and coupled quality factor by measuring the resonance linewidth and minimum transmission as a function of the gap. The spectra shown in Figs. 1(a) and 2 are obtained with resonators with intrinsic quality factors of approximately 1×10^6 and comb-generation threshold powers as low as 9 mW in the coupling waveguide. Ongoing experiments show that intrinsic Q factors up to approximately 3×10^6 and threshold powers of 1 mW are possible at 1064 nm.

We efficiently generate soliton microcombs by controlling the pump-resonator detuning at a rate faster than the resonator thermal dynamics [36–38]. This is done with an ultrafast electro-optic frequency-shifting technique similar to that reported in Ref. [20]. Here we use a standard lithium niobate waveguide Mach-Zehnder intensity modulator in place of the single-sideband, suppressed-carrier modulator. The output of the intensity modulator is passed to a polarization controller and amplified in an ytterbium-doped fiber amplifier before being coupled into the chip. The blue-detuned sideband frequency is tuned to resonance and then decreased by approximately 5 GHz in 100 ns. This rapid pump-frequency tuning technique minimizes the thermo-optic shift of the resonance frequency, which can destabilize the soliton. The red sideband and residual carrier are far detuned (by 20 or more resonator linewidths) from any resonances and do not adversely affect soliton generation. We filter out the pump light to monitor the generated comb power. The emergence of soliton microcombs from chaotic states as we vary the detuning is identified from the photodetected comb power, with an oscilloscope; see the trace in Fig. 1(b).

Optical spectra of single-soliton microcombs that we create are shown in Fig. 2(a). We present spectra for five Ws, spaced by 20 nm from W of 810 to W of 890 nm. The spectra are obtained with on-chip, single-sideband pump powers between 160 and 190 mW. The comb line corresponding to the pump laser is graphically suppressed for compact display of the data. Each spectrum features two prominent dispersive waves on either side of the pump-laser frequency. The long-wavelength DWs (LDWs) are in the telecom C and L band and the short-wavelength DWs (SDWs) are in the NIR 780-nm band. The LDW and SDW frequencies are plotted versus the W in Fig. 2(b) as red and blue diamonds, respectively. For comparison, we also present DW frequency measurements obtained with blue-detuned chaotic combs (solid circles). This thorough and unique comparison of microcomb spectra is enabled by precision fabrication of numerous devices and reliable soliton-microcomb generation. Our measurements of
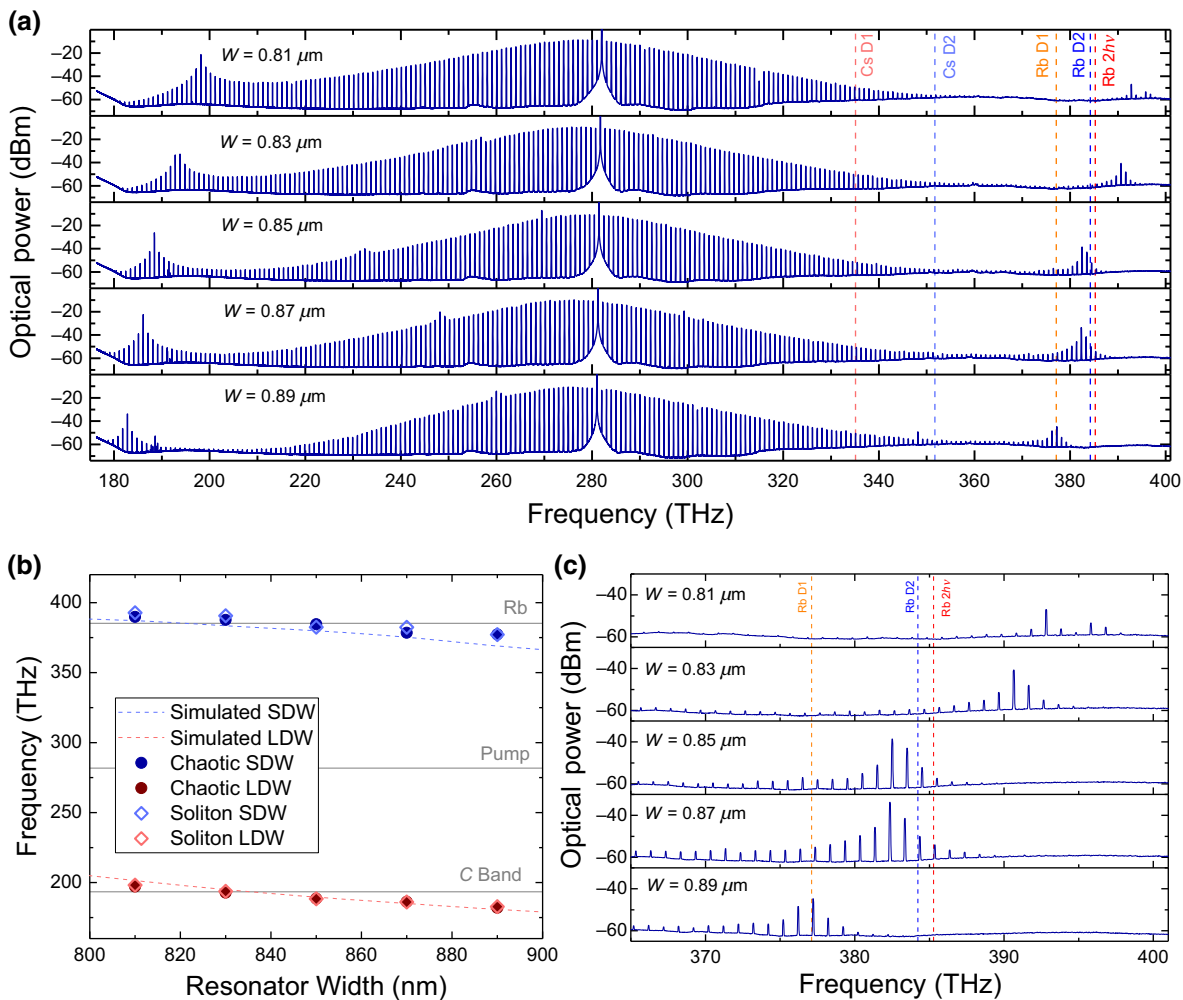
FIG. 2.   Soliton-microcomb-spectrum control through nanofabrication. (a) Single-soliton spectra obtained from resonators with various waveguide widths on the same chip. Relevant atomic transitions are indicated in the plot. The on-chip, single-sideband pump powers are, from top to bottom, 160, 180, 175, 190, and 160 mW. (b) Comparison between measured dispersive-wave frequencies and the frequency predicted by simulated waveguide dispersion showing good agreement within fabrication imprecision of resonator dimensions. (c) Enlarged plot near the rubidium optical transition frequencies.

the DW frequencies agree with our designs, which are based on finite-element calculations of D_{int} (open circles) using accurate Sellmeier coefficients for Si_3N_4 [39] and silica [40] and a fabrication precision that we assess to be approximately 20 nm. The predictability of dispersive-wave frequencies enables placement of dispersive waves on the targeted Rb resonances, as shown in the enlarged plot in Fig. 3(c).

We measure the repetition frequency of the soliton microcomb by electro-optic modulation of the LDW near 1550 nm. Such measurements are shown for the device with W of 830 nm in Fig. 3. This procedure creates a low-frequency (less than 100 MHz) optical heterodyne beat note f_{beat} that represents the 0.999291-THz repetition frequency. To facilitate these measurements, we use optical filters to isolate the dispersive waves near 1550 and 780 nm. The long-wavelength DW is amplified with

a C-band erbium-doped fiber amplifier, filtered, and sent to two electro-optic phase modulators operating in series and driven at $f_{EO} \approx 16.65$ GHz to create many coherent sidebands around each comb tooth [41]. We detect f_{beat} by photodetecting the phase-modulation sidebands nearly in between the two soliton-microcomb modes, allowing the repetition frequency to be determined via $f_{rep} = 60f_{EO} + f_{beat}$. A narrow-optical-bandpass filter selects the desired interfering modes [marked with an arrow in Fig. 3(a)] before photodetection of f_{beat}. The highly coherent beat obtained from this measurement [shown in Fig. 3(b)] confirms low-noise soliton operation.

We evaluate the frequency noise on individual comb modes by recording optical heterodyne beats between the soliton comb and an auxiliary low-noise cw laser. We focus on large comb mode numbers at a large frequency off-set from the 1064-nm pump laser, which are interesting
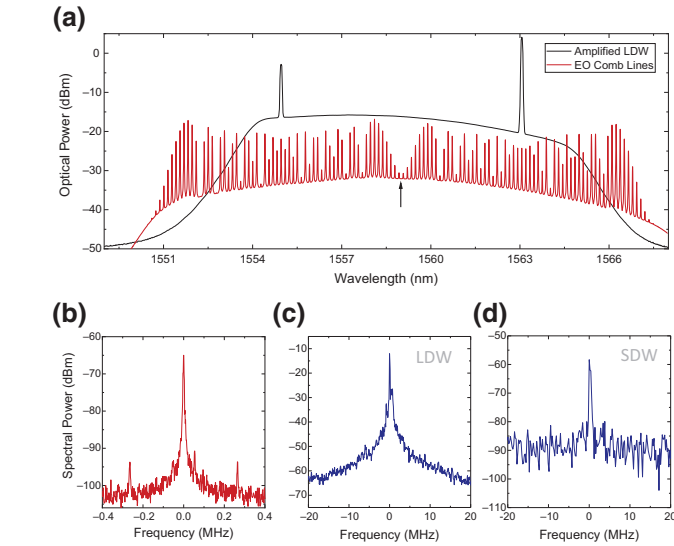
FIG. 3.   Soliton coherence measurements. (a) The filtered and amplified long-wavelength DW before (black) and after (red) being sent to electro-optic (EO) phase modulators. A heterodyne beat is made at the wavelength marked with an arrow to evaluate fluctuations in terahertz comb-mode spacing. This beat is shown in (b). (c,d) Heterodyne beats of each DW with a low-noise auxiliary laser: (c) LDW at 1563 nm and (d) SDW at 777.3 nm. The traces in (b)–(d) are taken with resolution bandwidth of 1, 100, and 300 kHz, respectively.

to test since they are most sensitive to multiplicative noise of the comb. A C-band external-cavity diode laser is heterodyned directly with the long-wavelength DW near 1563 nm, and it is also frequency doubled in a bulk periodically poled lithium niobate crystal for the short-wavelength DW near 777.3 nm. For both heterodyne beat notes, which are shown in Figs. 3(c) and 3(d) for the long-wavelength DW and the short-wavelength DW, respectively, we observe linewidths of a few megahertz that we associate with the linewidth of the soliton-microcomb modes. This is reasonable considering that the free-running repetition rate has a frequency linewidth of approximately 5 kHz and the comb modes we characterize in Figs. 3(c) and 3(d) are approximately 100 modes from the pump.

The DW wavelengths are chosen in this case to be near harmonic to facilitate f-$2f$ referencing. For this particular device, the offset frequency f_0 is approximately 80 ± 1 GHz. While such a high frequency makes a direct electronic measurement of f_0 challenging, in future designs we would systematically vary the resonator radius in steps of approximately 10 nm to create a specific device that satisfies the condition $f_0 \leq 20$ GHz [20].

IV. THERMO-OPTIC FINE-TUNING

We finely shift the absolute frequencies of the soliton-comb modes beyond the level provided by nanofabrication process control using thermo-optic tuning of the resonator.

This approach combines the high optical power per mode of DKS combs with the high spectral resolution typical of lower-repetition-rate combs [42]. The temperature of the chip is set with a feedback controlled thermoelectric heater; see Fig. 1(b) for the setup. Figures 4(a) and 4(b) show the thermal tuning of solitons created in resonators with a waveguide width of 870 nm [second-to-last panel in Figs. 2(a) and 2(c)]. Comb modes near 778 nm have a measured tuning coefficient of −5.48 GHz/°C, which is sufficiently large to access the Rb two-photon and D2 resonances at chip temperatures of approximately 37 °C and approximately 44 °C, respectively; see Fig. 4(a). The change in the comb modes' power between these two temperatures is associated with hysteresis in switching behavior between distinct operating regimes of the single-soliton pulse. This behavior is attributed to interference between phase-dependent, extended-cw-background and DW intensities similar to those in recent theoretical work [30] and experimental work [36] and will be explored in more detail in future work. The measured linear thermal tuning of the soliton repetition rate of 15.86 ± 0.34 MHz/°C shown in Fig. 4(b) amounts to a fractional change of approximately 16 ppm on the 1.0-THz spacing. This is in reasonable agreement with measured thermo-optic coefficients of bulk silicon nitride at 20–30 ppm [43] as well as experimental
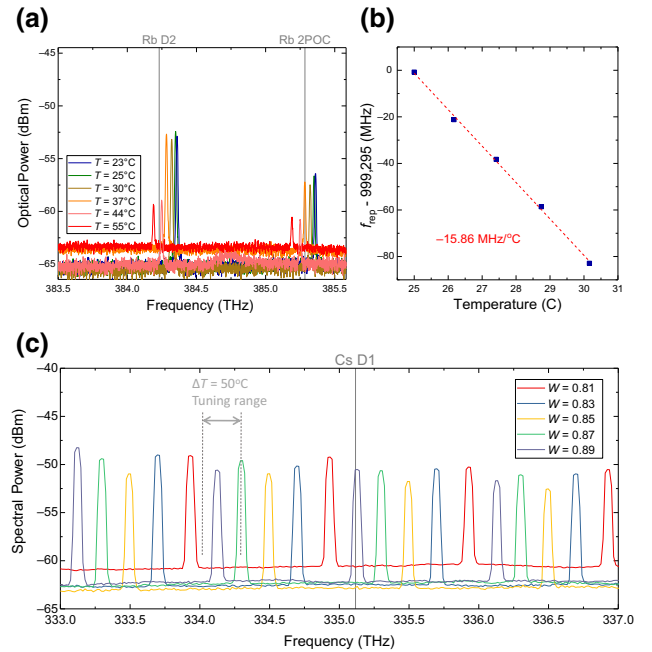

FIG. 4.   Thermo-optic tuning of soliton spectrum. (a) The thermal tuning of two modes of the soliton spectrum across the Rb two-photon optical clock transition (2POC) and Rb D2 transitions. (b) The repetition rate of the soliton can also be thermally tuned. (c) Overlay of the spectra presented in Fig. 2 plotted over the range from 333 to 337 THz. Any arbitrary frequency can be reached with the current W sweep and a 50-°C thermal tuning range.

measurements on resonators pumped at 1550 nm [44], with potentially a weak component from thermal expansion of the ring geometry with the same sign [45]. Temperature variations in the offset frequency can be approximated by $df_0/dT = (dn_g/dT - dn_p/dT)f_p/n_g$, where n_p and n_g are the phase and group indexes of refraction and f_p is the pump frequency [44]. Because dn_g/dT and dn_p/dT are of similar magnitude, temperature variations have a comparatively small effect on f_0. We plan to incorporate integrated heaters [44,46], which will reduce the overall electrical power consumption.

Through both lithographic variation in resonator dimensions and thermo-optic tuning, we exert comprehensive frequency control over the Si_3N_4 comb. A typical chip used in this study contains 70 devices, which is sufficient to include combinations of fine resonator width and gap sweeps for desired dispersion and coupling. A modest $\Delta T = 50\,^{\circ}C$ thermal-optic tuning of the chip is sufficient to place a comb line onto any desired wavelength within the design bandwidth of the resonators. For example, to probe the cesium D1 transition, we can select a device with W of 870 or 890 nm and thermally tune the modes toward lower frequency to align them with the desired transition, as shown in Fig. 4(c).

V. CONCLUSION

We present Kerr-soliton frequency combs operating in the near-infrared region using silicon nitride microresonators. Dispersion engineering of the resonator waveguide provides octave bandwidth through the emission of dual dispersive waves at predictable wavelengths on either side of the pump-laser wavelength. Further, our chosen design wavelengths for the pump laser as well as both the long-wavelength DW and the short-wavelength DW offer significant advantages for future compact comb systems. Pumping at 1064 nm allows robust generation of low-noise solitons using fast frequency sweeps from standard electro-optic intensity modulators. Full stabilization of the comb could be straightforwardly accomplished by leveraging the LDW's position in the telecom C and L band using mature optical technology such as erbium amplifiers, efficient second-harmonic generators, and optical modulators. The SDW is ideal for applications requiring high power per mode in the 760–900-nm NIR band. We demonstrate the flexibility of our system by thermally tuning optical comb modes to continuously fill in wide bandwidths across the near-infrared region and onto Rb and Cs resonances. This tunability will enable future experiments exploring spectroscopy and metrology with atomic resonances.

ACKNOWLEDGMENTS

[1] David J. Moss, Roberto Morandotti, Alexander L. Gaeta, and Michal Lipson, New CMOS-compatible platforms based on silicon nitride and Hydex for nonlinear optics, Nat. Photonics **7,** 597 (2013).

[2] Jiang Li, Hansuek Lee, and Kerry J. Vahala, Microwave synthesizer using an on-chip Brillouin oscillator, Nat. Commun. **4,** 2097 (2013).

[3] William Loh, Adam A. S. Green, Fred N. Baynes, Daniel C. Cole, Franklyn J. Quinlan, Hansuek Lee, Kerry J. Vahala, Scott B. Papp, and Scott A. Diddams, Dual-microcavity narrow-linewidth Brillouin laser, Optica **2,** 225 (2015).

[4] David R. Carlson, Daniel D. Hickstein, Alex Lind, Stefan Droste, Daron Westly, Nima Nader, Ian Coddington, Nathan R. Newbury, Kartik Srinivasan, Scott A. Diddams, and Scott B. Papp, Self-referenced frequency combs using high-efficiency silicon-nitride waveguides, Opt. Lett. **42,** 2314 (2017).

[5] Erin S. Lamb, David R. Carlson, Daniel D. Hickstein, Jordan R. Stone, Scott A. Diddams, and Scott B. Papp, Optical-Frequency Measurements with a Kerr Microcomb and Photonic-Chip Supercontinuum, Phys. Rev. Appl. **9,** 024030 (2018).

[6] T. Herr, V. Brasch, J. D. Jost, C. Y. Wang, N. M. Kondratiev, M. L. Gorodetsky, and T. J. Kippenberg, Temporal solitons in optical microresonators, Nat. Photonics **8,** 145 (2014).

[7] Tobias J. Kippenberg, Alexander L. Gaeta, Michal Lipson, and Michael L. Gorodetsky, Dissipative Kerr solitons in optical microresonators, Science **361,** eaan8083 (2018).

[8] Chengying Bao, Jose A. Jaramillo-Villegas, Yi Xuan, Daniel E. Leaird, Minghao Qi, and Andrew M. Weiner, Observation of Fermi-Pasta-Ulam Recurrence Induced by Breather Solitons in an Optical Microresonator, Phys. Rev. Lett. **117,** 163901 (2016).

[9] Erwan Lucas, Maxim Karpov, H. Guo, M. L. Gorodetsky, and Tobias J. Kippenberg, Breathing dissipative solitons in optical microresonators, Nat. Commun. **8,** 736 (2017).

[10] Mengjie Yu, Jae K. Jang, Yoshitomo Okawachi, Austin G. Griffith, Kevin Luke, Steven A. Miller, Xingchen Ji, Michal Lipson, and Alexander L. Gaeta, Breather soliton dynamics in microresonators, Nat. Commun. **8,** 14569 (2017).

[11] Xiaoxiao Xue, Yi Xuan, Yang Liu, Pei-Hsun Wang, Steven Chen, Jian Wang, Dan E. Leaird, Minghao Qi, and Andrew M. Weiner, Mode-locked dark pulse Kerr combs in normal-dispersion microresonators, Nat. Photonics **9,** 594 (2015).

[12] Daniel C. Cole, Erin S. Lamb, Pascal Del'Haye, Scott A. Diddams, and Scott B. Papp, Soliton crystals in Kerr resonators, Nat. Photonics **11,** 671 (2017).

[13] Pablo Marin-Palomo, Juned N. Kemal, Maxim Karpov, Arne Kordts, Joerg Pfeifle, Martin H. P. Pfeiffer, Philipp Trocha, Stefan Wolf, Victor Brasch, Miles H. Anderson, Ralf Rosenberger, Kovendham Vijayan, Wolfgang Freude, Tobias J. Kippenberg, and Christian Koos, Microresonator-based solitons for massively parallel coherent optical communications, Nature **546,** 274 (2017).

[14] Daryl T. Spencer *et al.*, An optical-frequency synthesizer using integrated photonics, Nature **557,** 81 (2018).

[15] Xu Yi, Qi-Fan Yang, Ki Youl Yang, Myoung-Gyun Suh, and Kerry Vahala, Soliton frequency comb at microwave rates in a high-*Q* silica microresonator, Optica **2,** 1078 (2015).

[16] Yadong Wang, Francois Leo, Julien Fatome, Miro Erkintalo, Stuart G. Murdoch, and Stéphane Coen, Universal mechanism for the binding of temporal cavity solitons, Optica **4,** 855 (2017).

[17] Andrey B. Matsko, Wei Liang, Anatoliy A. Savchenkov, Danny Eliyahu, and Lute Maleki, Optical Cherenkov radiation in overmoded microresonators, Opt. Lett. **41,** 2907 (2016).

[18] Victor Brasch, Michael Geiselmann, Tobias Herr, Grigoriy Lihachev, Martin H. P. Pfeiffer, Michael L. Gorodetsky, and Tobias J. Kippenberg, Photonic chip–based optical frequency comb using soliton Cherenkov radiation, Science **351,** 357 (2016).

[19] Jose A. Jaramillo-Villegas, Xiaoxiao Xue, Pei-Hsun Wang, Daniel E. Leaird, and Andrew M. Weiner, Deterministic single soliton generation and compression in microring resonators avoiding the chaotic region, Opt. Express **23,** 9618 (2015).

[20] Travis C. Briles, Jordan R. Stone, Tara E. Drake, Daryl T. Spencer, Connor Fredrick, Qing Li, Daron Westly, B. R. Ilic, Kartik Srinivasan, Scott A. Diddams, and Scott B. Papp, Interlocking Kerr-microresonator frequency combs for microwave to optical synthesis, Opt. Lett. **43,** 2933 (2018).

[21] Brian Stern, Xingchen Ji, Yoshitomo Okawachi, Alexander L. Gaeta, and Michal Lipson, Battery-operated integrated frequency comb generator, Nature **562,** 401 (2018).

[22] Scott B. Papp, Katja Beha, Pascal Del'Haye, Franklyn Quinlan, Hansuek Lee, Kerry J. Vahala, and Scott A. Diddams, Microresonator frequency comb optical clock, Optica **1,** 10 (2014).

[23] Z. L. Newman, Photonic integration of an optical atomic clock, arXiv:1811.00616 (2018).

[24] Maxim Karpov, Martin H. P. Pfeiffer, Junqiu Liu, Anton Lukashchuk, and Tobias J. Kippenberg, Photonic chip-based soliton frequency combs covering the biological imaging window, Nat. Commun. **9,** 1146 (2018).

[25] Imad H. Agha, Yoshitomo Okawachi, and Alexander L. Gaeta, Theoretical and experimental investigation of broadband cascaded four-wave mixing in high-*Q* microspheres, Opt. Express **17,** 16209 (2009).

[26] Yoshitomo Okawachi, Michael R. E. Lamont, Kevin Luke, Daniel O. Carvalho, Mengjie Yu, Michal Lipson, and Alexander L. Gaeta, Bandwidth shaping of microresonator-based frequency combs via dispersion engineering, Opt. Lett. **39,** 3535 (2014).

[27] Scott A. Diddams, James C. Bergquist, Steven R. Jefferts, and Christopher W. Oates, Standards of time and frequency

at the outset of the 21st century, Science **306,** 1318 (2004).

[28] Andrew D. Ludlow, Martin M. Boyd, Jun Ye, Ekkehard Peik, and Piet O. Schmidt, Optical atomic clocks, Rev. Mod. Phys. **87,** 637 (2015).

[29] R. Le Targat *et al.*, Experimental realization of an optical second with strontium lattice clocks, Nat. Commun. **4,** 2109 (2013).

[30] D. V. Skryabin and Y. V. Kartashov, Self-locking of the frequency comb repetition rate in microring resonators with higher order dispersions, Opt. Express **25,** 27442 (2017).

[31] L. Hilico, R. Felder, D. Touahri, O. Acef, A. Clairon, and F. Biraben, Metrological features of the rubidium two-photon standards of the BNM-LPTF and Kastler Brossel laboratories, Eur. Phys. J. Appl. Phys. **4,** 219 (1998).

[32] Nathan D. Zameroski, Gordon D. Hager, Christopher J. Erickson, and John H. Burke, Pressure broadening and frequency shift of the $5S_{1/2} \rightarrow 5D_{5/2}$ and $5S_{1/2} \rightarrow 7S_{1/2}$ two photon transitions in ^{85}Rb by the noble gases and N$_2$, J. Phys. B: At, Mol. Opt. Phys. **47,** 225205 (2014).

[33] J. E. Bernard, A. A. Madej, K. J. Siemsen, L. Marmet, C. Latrasse, D. Touahri, M. Poulin, M. Allard, and M. Têtu, Absolute frequency measurement of a laser at 1556 nm locked to the $5S_{1/2}$-$5D_{5/2}$ two-photon transition in ^{87}Rb, Opt. Commun. **173,** 357 (2000).

[34] Ehsan Shah Hosseini, Siva Yegnanarayanan, Amir Hossein Atabaki, Mohammad Soltani, and Ali Adibi, Systematic design and fabrication of high-*Q* single-mode pulley-coupled planar silicon nitride microdisk resonators at visible wavelengths, Opt. Express **18,** 2127 (2010).

[35] Qing Li, Travis C. Briles, Daron Westly, Jordan Stone, Robert Ilic, Scott Diddams, Scott Papp, and Kartik Srinivasan, in *Frontiers in Optics* (Optical Society of America, San Jose, California, USA, 2015), p. FW6C–5.

[36] Travis C. Briles, Jordan R. Drake, Daryl T. Spencer, Connor Frederick, Qing Li, Daron A. Westly, B. Robert Illic, Kartik Srinivasan, Scott A. Diddams, and Scott B. Papp, Kerr-microresonator solitons for accurate carrier-envelope-frequency stabilization, arXiv:1711.06251 (2017).

[37] Jordan R. Stone, Travis C. Briles, Tara E. Drake, Daryl T. Spencer, David R. Carlson, Scott A. Diddams, and Scott B. Papp, Thermal and Nonlinear Dissipative-Soliton Dynamics in Kerr-Microresonator Frequency Combs, Phys. Rev. Lett. **121,** 063902 (2018).

[38] Qing Li, Travis C. Briles, Daron A. Westly, Tara E. Drake, Jordan R. Stone, B. Robert Ilic, Scott A. Diddams, Scott B. Papp, and Kartik Srinivasan, Stably accessing octave-spanning microresponator frequency combs in the soliton regime, Optica **4,** 193 (2017).

[39] Kevin Luke, Yoshitomo Okawachi, Michael R. E. Lamont, Alexander L. Gaeta, and Michal Lipson, Broadband mid-infrared frequency comb generation in a Si$_3$N$_4$ microresonator, Opt. Lett. **40,** 4823 (2015).

[40] I. H. Malitson, Interspecimen comparison of the refractive index of fused silica, J. Opt. Soc. Am. **55,** 1205 (1965).

[41] Pascal Del'Haye, Scott B. Papp, and Scott A. Diddams, Hybrid electro-optically Modulated Microcombs, Phys. Rev. Lett. **109,** 263901 (2012).

[42] D. C. Heinecke, A. Bartels, T. M. Fortier, D. A. Braje, L. Hollberg, and S. A Diddams, Optical frequency

stabilization of a 10 Ghz Ti:sapphire frequency comb by saturated absorption spectroscopy in rubidium 87, Phys. Rev. A **80**, 053806 (2009).

[43] Kazuhiro Ikeda, Robert E. Saperstein, Nikola Alic, and Yeshaiahu Fainman, Thermal and Kerr nonlinear properties of plasma-deposited siliconnitride/silicon dioxide waveguides, Opt. Express **16**, 12987 (2008).

[44] Xiaoxiao Xue, Yi Xuan, Cong Wang, Pei-Hsun Wang, Yang Liu, Ben Niu, Daniel E. Leaird, Minghao Qi, and Andrew M. Weiner, Thermal tuning of Kerr frequency combs in silicon nitride microring resonators, Opt. Express **24**, 687 (2016).

[45] Amit Kaushik, Harold Kahn, and Arthur H. Heuer, Wafer-level mechanical characterization of silicon nitride MEMS, Opt. Lett. **41**, 359 (2016).

[46] Chaitanya Joshi, Jae K. Jang, Kevin Luke, Xingchen Ji, Steven A. Miller, Alexander Klenner, Yoshitomo Okawachi, Michal Lipson, and Alexander L. Gaeta, Thermally controlled comb generation and soliton modelocking in microresonators, Opt. Lett. **41**, 2565 (2016).